Original Research *Highlight article*

The novel potential biomarkers for multidrug-resistance tuberculosis using UPLC-Q-TOF-MS

Huai Huang[1,2], Yu-Shuai Han[1,3], Jing Chen[1,3], Li-Ying Shi[4], Li-Liang Wei[5], Ting-Ting Jiang[1,3], Wen-Jing Yi[1,3], Yi Yu[6], Zhi-Bin Li[1,3] and Ji-Cheng Li[1,3]

[1]Medical Research Center, Yue Bei People's Hospital, Shaoguan 512025, China; [2]School of Medicine, South China University of Technology, Guangzhou, 510006, China; [3]Institute of Cell Biology, Zhejiang University, Hangzhou 310058, China; [4]Department of Clinical Laboratory, Zhejiang Hospital, Hangzhou 310013, China; [5]Department of Pneumology, Shaoxing University Affiliated Hospital, Shaoxing 312099, China; [6]College of Chemical Engineering, Zhejiang University of Technology, Hangzhou 310014, China
Corresponding author: Ji-Cheng Li. Email: lijichen@zju.edu.cn

Impact statement

The MDR-TB incidence remains high, making the effective control of TB epidemic yet challenging. Rapid and accurate diagnosis is vitally important for improving the therapeutic efficacy and controlling the prevalence of drug resistance TB. Metabolomics has dramatic potential to distinguish MDR-TB and DS-TB. N1M2P5C, MG3P, CA, and DX that we identified in this study might have potential as novel MDR-TB biomarkers. The phospholipid remodeling of cell membranes was highly active in MDR-TB. The DPPC metabolites in TB were significantly down-regulated. This work aimed to investigate potential MDR-TB biomarkers to enhance the clinical diagnostic efficacy. The metabolic pathway distinctly altered in MDR-TB might provide novel targets to develop new anti-TB drugs.

Abstract

The lack of rapid and efficient diagnostics impedes largely the epidemic control of multidrug-resistant tuberculosis, and might misguide the therapeutic strategies as well. This study aimed to identify novel multidrug-resistant tuberculosis biomarkers to improve the early intervention, symptomatic treatment and control of the prevalence of multidrug-resistant tuberculosis. The serum small molecule metabolites in healthy controls, patients with drug-susceptible tuberculosis, and patients with multidrug-resistant tuberculosis were screened using ultra-high-performance liquid chromatography combined with quadrupole-time-of-flight mass spectrometry (UPLC-Q-TOF-MS). The differentially abundant metabolites were filtered out through multidimensional statistical analysis and bioinformatics analysis. Compared with drug-susceptible tuberculosis patients and healthy controls, the levels of 13 metabolites in multidrug-resistant tuberculosis patients altered. Among them, the most significant changes were found in N1-Methyl-2-pyridone-5-carboxamide (N1M2P5C), 1-Myristoyl-sn-glycerol-3-phosphocholine (MG3P), Caprylic acid (CA), and D-Xylulose (DX). And a multidrug-resistant tuberculosis/drug-susceptible tuberculosis differential diagnostic model was built based on these four metabolites, achieved the accuracy, sensitivity, and specificity of 0.928, 86.7%, and 86.7%, respectively. The enrichment analysis of metabolic pathways showed that the phospholipid remodeling of cell membranes was active in multidrug-resistant tuberculosis patients. In addition, in patients with tuberculosis, the metabolites of dipalmitoyl phosphatidylcholine (DPPC), a major component of pulmonary surfactant, were down-regulated. N1M2P5C, MG3P, CA, and DX may have the potential to serve as novel multidrug-resistant tuberculosis biomarkers. This research provides a preliminary experimental basis to further investigate potential multidrug-resistant tuberculosis biomarkers.

Keywords: Multidrug-resistance tuberculosis, potential biomarkers, metabolomics, serum, phospholipid remodeling, drug-sensitive tuberculosis

Experimental Biology and Medicine **2020; 245: 501–511. DOI: 10.1177/1535370220903464**

Introduction

Multidrug-resistant tuberculosis (MDR-TB) is defined as tuberculosis (TB) that is resistant to isoniazid and rifampicin, the two most effective anti-TB drugs, which are infected by multidrug-resistant *Mycobacterium tuberculosis* (MDR-MTB). MDR-TB has characteristics of low awareness rate (25%), difficult treatment (second-line medication), long treatment period (at least 18 months), low cure rate

(55%), and high mortality (15%),[1] compared to drug-sensitive tuberculosis (DS-TB), which can directly lead to the widespread of TB and the failure of anti-TB treatment. With a high incidence and low detection efficiency, China is one of the most MDR-TB burdened countries. In 2017, the number of new MDR/RR-TB (rifampicin-resistance tuberculosis) cases in China accounted for 13% of the global MDR/RR-TB cases, ranking as the second in the world.[1] However, the MDR/RR-TB discovery rate in China was only 19%, which was much lower than the global average rate (29%).[1] Therefore, improving the diagnostic efficiency of MDR-TB for the control of the TB epidemic has been regarded as the primary task.

However, the present clinical diagnosis of MDR-TB is underdeveloped and the detection efficiency is low. In 2017, globally only 24% of new TB cases were tested for anti-rifampicin.[1] Currently, the drug susceptibility testing (DST) is still considered as the MDR-TB clinical diagnostic gold standard. While DST may take three to eight weeks,[2] which can obstruct the timely adjustment of drug regimens. Moreover, the DST detection rate in Europe (where DST detection coverage is the highest) was only 57%, while China had an even lower detection rate of 45%.[1] The molecular biology-based rapid diagnosis, Xpert MTB/RIF® test can diagnosis TB within 90 min, but it can only diagnose the resistance to rifampicin and requires a high sputum load.[3] The diagnostic sensitivity and specificity of the above methods get a significant decrease in non-open or sputum-negative TB patients, which may delay the early identification of MDR-TB. Therefore, it is urgent to identify novel MDR-TB biomarkers with a high sensitivity and specificity.

Previously, our laboratory studied differentially altered proteins and miRNAs in MTB patients by Solexa sequencing and iTRAQ-2D LC-MS/MS.[4] However, the interactions between pathogens and the host body are the basis for the progression of the disease, while the dynamics of the interactions between MDR-MTB and the host cannot be predicted by transcriptomics and proteomics.[5] Metabolites are downstream products that are co-regulated by endogenous and exogenous substrates, representing the amplified expression changes of upstream genes and proteins.[6] Meanwhile, metabolites can also reflect the interactions between the genetic materials and the external environment and are more sensitive to individualized differentiation.[7,8] In addition, biochemical feedback loops and cyclic processes are commonly found in biological systems, where the changes in metabolite concentrations can alter gene and protein function.[9] Therefore, the study of characteristic metabolites and metabolic pathways could help us further understand the heterogeneity of MDR-TB and the potential response to treatment.

This study was the first to use ultra-performance liquid chromatography combined with quadrupole-time-of-flight mass spectrometry (UPLC-Q-TOF-MS) to screen serum differential metabolites between healthy controls (HC), DS-TB patients, and MDR-TB patients. Potential serum biomarkers and characteristic MDR-TB metabolic profiles were obtained. This research may provide preliminary experimental data to identify potential biomarkers of MDR-TB and deepen the understanding of the pathogenic mechanism between MDR-MTB and the host.

Material and methods

Clinical subjects

According to the criteria issued by the National Health Commission of the People's Republic of China,[10] subjects were diagnosed with TB if they meet one of the following criteria: 1. Positive sputum test (① Two sputum samples were positive under microscopy. ② One sputum sample was positive under microscopy, with typical chest imaging changes. ③ One sputum sample was positive under microscopy and one for mycobacterial culture). 2. Negative sputum test, but two mycobacterial cultures were positive, with typical chest imaging changes. 3. Molecular biology examination positive for TB with typical imaging chest changes. 4. The lung specimen presented a pathological change of TB. 5. Excluding tracheal or bronchial TB or tuberculous pleurisy. Each TB patient was diagnosed with MDR-TB or DS-TB after more than two DST for the *Mycobacterium tuberculosis* complex (MTBC). Patients with extrapulmonary TB, HIV infection, malignant tumors, autoimmune diseases, and chronic metabolic diseases were excluded.

Between September 2013 and April 2019, the MDR-TB and DS-TB subjects were enrolled from the First Affiliated Hospital of Jiaxing University and Shaoxing University Affiliated Hospital (China), respectively. Additionally, from the Zhejiang Hospital (China), the HC without TB and other concomitant diseases were recruited. Regardless of age or gender, there were no statistically significant differences between three groups (Table 1).

Table 1. Characteristics of the MDR-TB patients, DS-TB patients, and health controls.

	MDR-TB patients (*N*=30)	DS-TB patients (*N*=30)	HC (*N*=30)	*P*-value
Age (mean ± SD)	41.46 ± 13.84	37.47 ± 14.21	37.67 ± 11.29	0.4358[a]
Gender (male/female)	19/11	22/8	16/14	0.2748[b]
Positive sputum smear (%)	30 (100%)	22 (73.33%)	/	/
Lung lesion (single/double)	6/24	17/13	/	/
Chest X-ray cavity (%)	12 (40%)	8 (26.67%)	/	/

[a]*P*-value among three groups from one-way analysis of variance (ANOVA) test.
[b]*P*-value among three groups from the Chi-square test.
N: number of subjects; MDR-TB: multidrug-resistant tuberculosis; DS-TB: drug-sensitive tuberculosis; HC: health controls.

The morning fasting peripheral blood was collected from all subjects. After the blood sample was taken, the supernatant was separated within 1 h, and placed at −80°C.

Metabolite extraction and UPLC-Q-TOF-MS detection

The serum sample was slowly dissolved at 4°C; 400 μL of pre-cooled methanolic acetonitrile (1:1, v/v) was added into 100 μL serum sample. After that, sample was vortexed for 60 s, and the precipitated protein was placed for 1 h at 20°C. Subsequently, the sample was centrifuged for 20 min, at 14,000 rcf, 4°C. The supernatant was lyophilized and stored at −80°C.[11] In addition, samples of an equal amount were mixed to prepare quality control samples, and the treatment method was the same as described above.

The UPLC system (1290 Infinity LC, Agilent) was used to separate metabolites. The flow rate and the column temperature were 0.3 mL/min and 25°C, respectively. The reagents and experiment settings were employed by HILIC column (2.1 mm × 100 mm, ACQUITY UPLC BEH Amide 1.7 μm, Waters). The composition of mobile phase A was 25 mM ammonia + 25 mM ammonium acetate + water, and B was acetonitrile. Gradient elution procedure: During 0–1 min, B was 95%. During 1–14 min, B was linearly changed from 95% to 65%. During 14–16 min, B was linearly changed from 65% to 40%. During 16–18 min, B was maintained at 40%. During 18–18.1 min, B was linearly changed from 40% to 95%. During 18.1–23 min, B was maintained at 95%. Electrospray ionization (ESI) source parameters after HILIC chromatographic separation: Curtain gas (CUR) was 30, Ion Source Gas1 (Gas1) and Ion Source Gas2 (Gas2) were both 60, IonSapary Voltage Floating (ISVF) was ±5500 V, and source temperature (ST) was 600°C (positive/negative ion mode).

The reagents and experiment settings were employed by HSS T3 column (2.1 × 100 mm, ACQUITY UPLC HSS T3 1.8 μm, Waters). The composition mobile phase of positive ion mode: A was 0.1% aqueous formic acid, and B was 0.1% formic acid acetonitrile. The composition mobile phase of negative ion mode: A was 0.5 mM aqueous ammonium fluoride solution, and B was acetonitrile. Gradient elution procedure: During 0–1.5 min, B was 1%. During 1.5–13 min, B was varied linearly from 1% to 99%. During 13–16.5 min, B was maintained at 99%. During 16.5–16.6 min, B was linear from 99% change to 1%. During 16.6–20 min, B was maintained at 1%. ESI source parameters (positive/negative ion mode) after HSS T3 chromatographic separation: CUR was 30, Gas1 was 40, Gas2 was 80, ISVF was ±5000 V, and ST was 650°C.

The AB Triple TOF 5600 mass spectrometer (AB SCIEX) was applied to mass spectrometry analysis of samples. The scan m/z range of product ion and TOF MS was 25–1000 Da and 60–1000 Da, respectively. And the scan accumulation time of product ion and TOF MS was 0.05 s/spectra and 0.20 s/spectra, respectively. Then, information-dependent acquisition (IDA) for obtaining the secondary mass spectrum was set up as follows: Candidate ions to monitor per cycle were 6, and exclude isotope was within 4 Da. Collision energy was 35 ±15 eV and Declustering potential (DP) was ±60 V.[12]

Data adjustment and statistical analysis

ProteoWizard was applied to convert raw data to .mzXML format. Peakview (V1.2) was used to perform the retention time correction, peak alignment, and peak area extraction. The secondary spectral matching was used to identify metabolite structure in conjunction with accurate mass-matching (<25 ppm) and an internal MS/MS database. After preprocessing the data with Pareto-scaling, SIMCA software (V14.1) was applied to multidimensional statistical analysis. Principal component analysis (PCA) and orthogonal projections to latent structures-discriminant analysis (OPLS-DA) were performed in sequence. Meanwhile, the variable importance in projection (VIP) values was calculated. The model validity was evaluated by 7-fold cross-validation and permutation test ($n = 200$).

SPSS software (V16.0) was used to perform statistical analysis, and P value <0.05 was recognized as statistically significant. One-way analysis of variance (ANOVA) was applied to calculate the parameter data of the three groups, and the composition ratio was tested by Chi-square test. Student's t-test was used for single-dimensional statistical analysis. The volcano map was drawn by R software. GraphPad Prism 5 was applied to draw scatter plots. Through the reference database of Kyoto Encyclopedia of Genes and Genomes (KEGG), the metabolic pathway was analyzed. MedCalc software (V12.4.2.0) was used to calculate the receiver operating characteristic (ROC) curve.

Results

Raw mass spectrometry data preprocessing

The raw mass spectral data were processed by peak labeling, baseline filtering, retention time correction, normalization, and other standard procedures. For HILIC columns, in the positive and negative spectrum mode, 7810 and 5497 characteristic ion peaks were detected, respectively. For T3 columns, in positive and negative spectral mode, 7592 and 5250 characteristic ion peaks were detected, respectively.

Difference in MDR-TB/DS-TB group

After multivariate pattern recognition analysis by PCA and OPLS-DA, the distinct metabolic profiles of MDR-TB different from DS-TB were obtained. The scores for OPLS-DA analysis of the HILIC column and the T3 column showed that the model could clearly distinguish between MDR-TB and DS-TB (Figures 1(a) and (c) and 2(a) and (c)). The model stability was further evaluated through the permutation test. The results showed that the model did not have over-fitting and obtained a good predictive performance (Figures 1(b) and (d) and 2(b) and (d)), and the parameters are shown in Table 2. Therefore, it could be reliably used to screen biomarkers.

Then according to the VIP values of OPLS-DA, the variables that distinguished between DS-TB and MDR-TB,

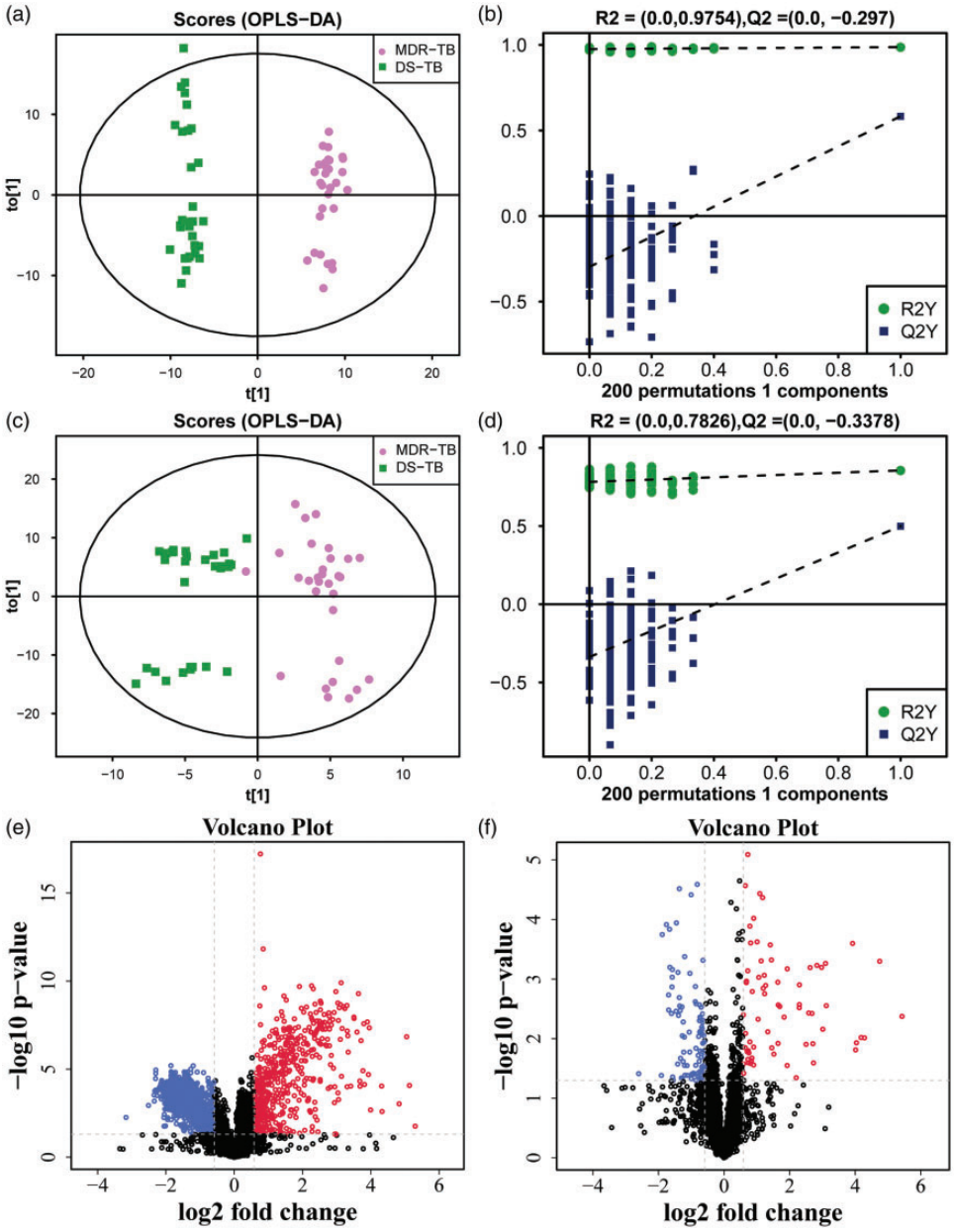

Figure 1. The OPLS-DA model and volcano map of MDR-TB/DS-TB group in HILIC column. The OPLS-DA score scatter plots of ion mode: (a) positive, (c) negative. The permutation test results of ion mode: (b) positive, (d) negative. The differential metabolite volcano maps of ion mode: (e) positive, (f) negative. The upward trend in metabolites was indicated by red scatters, the downward trend in metabolites was indicated by blue scatters, and the non-significant trend in metabolites was indicated by black scatters. (A color version of this figure is available in the online journal.)

evidenced by VIP > 1, were selected. Between the two groups, the Student's *t*-test was performed and a substance with $P < 0.05$ was further selected. The screening results were shown in the volcano map (Figures 1(e) and (f) and 2(e) and (f)). Subsequently, a primary matching analysis of the mass spectrum peaks was performed on the primary screening material with VIP > 1 and $P < 0.05$. Among MDR-TB/DS-TB, a total of 32 differentially metabolites were screened, in which 14 were down-regulated and 18 were up-regulated (Supplementary Table 1). In addition, the enrichment analysis of KEGG pathway was applied in the identified differential metabolites. The results showed that metabolic pathways such as Choline metabolism in cancer and Biosynthesis of unsaturated fatty acids were over-represented by differential metabolites (Figure 3).

Difference in MDR-TB/HC group

Similarly, the score map for the OPLS-DA analysis showed that the model could distinguish between HC and MDR-TB clearly (Supplementary Figures 1(a) and (c) and 2(a) and (c)). The model was then subjected to the permutation test. The results also demonstrated that the OPLS-DA model did not have over-fitting, had a good predictive performance and a potential to be applied to screen biomarkers (Table 2, Supplementary Figures 1(b) and (d) and 2(b) and (d)). Similarly, a quadratic matching analysis of the mass spectral

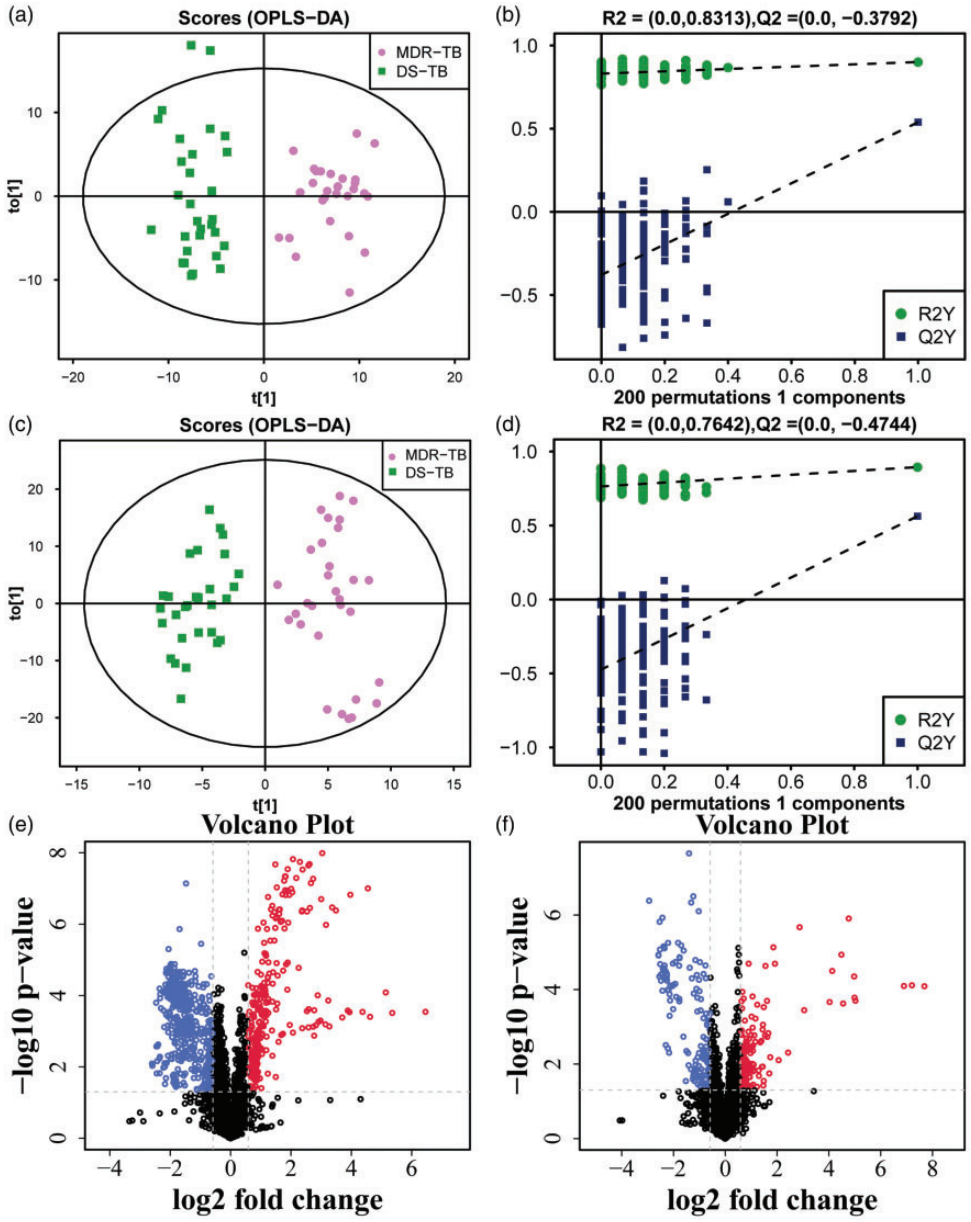

Figure 2. The OPLS-DA model and volcano map of MDR-TB/DS-TB group in T3 column. The OPLS-DA score scatter plots of ion mode: (a) positive, (c) negative. The permutation test results of ion mode: (b) positive, (d) negative. The differential metabolite volcano maps of ion mode: (e) positive, (f) negative. The upward trend in metabolites was indicated by red scatters, the downward trend in metabolites was indicated by blue scatters, and the non-significant trend in metabolites was indicated by black scatters. (A color version of this figure is available in the online journal.)

peaks was performed on the differential substances based on the thresholds of VIP >1 and $P<0.05$ (Supplementary Figures 1(e) and (f) and 2(e) and (f)). Among MDR-TB/HC, a total of 62 differentially metabolites were screened, in which 46 were down-regulated and 16 were up-regulated (Supplementary Table 2). Moreover, KEGG pathway enrichment analysis revealed that metabolic pathways such as retrograde endocannabinoid signaling and protein digestion and absorption were overrepresented by the differentially expressed proteins (Supplementary Figure 3).

Difference in DS-TB/HC group

Similarly, the score map for the OPLS-DA analysis showed that the model could distinguish between HC and DS-TB clearly (Supplementary Figures 4(a) and (c) and 5(a) and (c)). With regard to the predictive robustness, this model performed similarly to the first two models (Table 2, Supplementary Figures 4(b) and (d) and 5(b) and (d)). Again, based on a threshold of VIP >1 and $P<0.05$, the differential substances were screened and subsequently the mass spectral matching was performed (Supplementary Figures 4(e) and (f) and 5(e) and (f)). Among DS-TB/HC, a total of 63 differential metabolites were screened, in which 42 were down-regulated and 21 were up-regulated (Supplementary Table 3). In addition, the enrichment analysis of KEGG pathway revealed that metabolic pathways such as Central carbon metabolism in cancer and Linoleic acid metabolism occupied a

Table 2. Permutation test parameters of the OPLS-DA models.

	Column	Ion mode	R^2X	R^2Y	Q^2
MDR-TB/DS-TB group	HILIC	POS	0.550	0.987	0.583
		NEG	0.308	0.856	0.499
	T3	POS	0.428	0.901	0.539
		NEG	0.472	0.895	0.563
MDR-TB/HC group	HILIC	POS	0.394	0.980	0.897
		NEG	0.300	0.886	0.755
	T3	POS	0.234	0.904	0.830
		NEG	0.514	0.934	0.651
DS-TB/HC group	HILIC	POS	0.498	0.982	0.845
		NEG	0.403	0.976	0.781
	T3	POS	0.380	0.952	0.821
		NEG	0.461	0.927	0.651

POS: positive; NEG: negative; R^2X: the interpretability of the model for the categorical variable X; R^2Y: the interpretability of the model for the categorical variable Y; Q^2 values: predictability of the model; MDR-TB: multidrug-resistance tuberculosis; DS-TB: drug-sensitive tuberculosis; HC: health control.

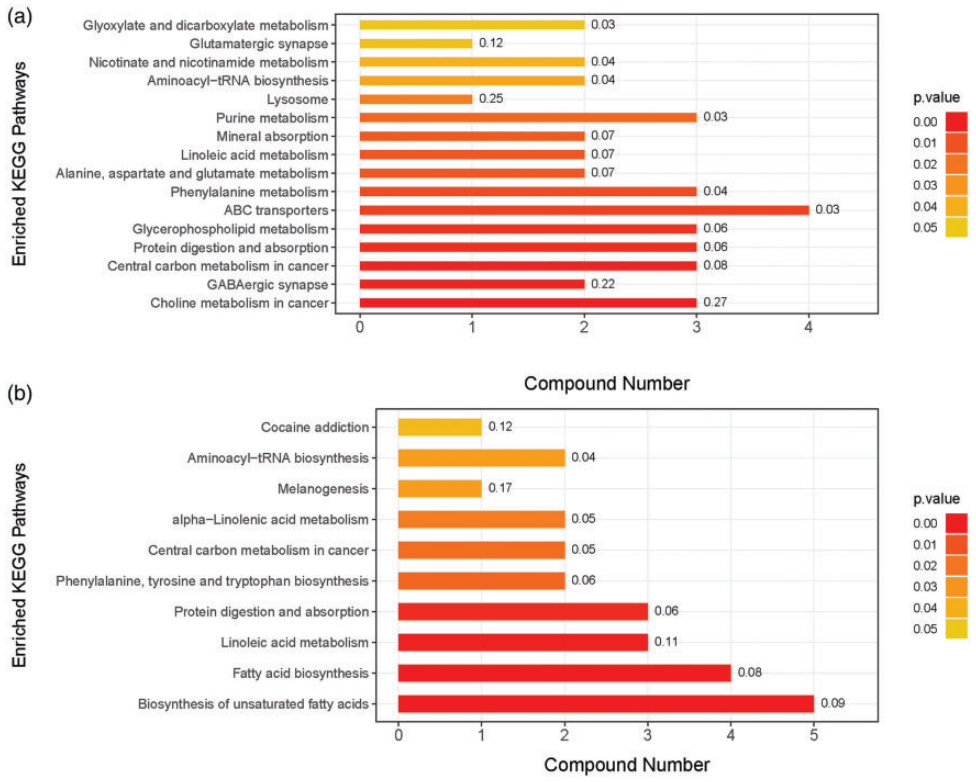

Figure 3. The metabolic pathway map of MDR-TB/DS-TB group. Metabolic pathway map of HILIC column (a), metabolic pathway map of T3 column (b). (A color version of this figure is available in the online journal.)

great advantage in differential metabolic pathways (Supplementary Figure 6).

Screening for differential metabolites of MDR-TB

Thirteen characteristic metabolites in MDR-TB were identified by comparing to HC and DS-TB based on the threshold of $P < 0.05$ and VIP > 1 (Table 3). Subsequently, through metabolic pathway analysis, it was found that a series of differentially down-regulated metabolites were concentrated in the stearoylcholine metabolic pathway. In addition, it was also found that the metabolites of dipalmitoyl phosphatidylcholine (DPPC), the main component of pulmonary surfactant, were also down-regulated in TB patients compared to HC (Figure 4).

Next, according to fold change >1.3 or <0.7, VIP >1.3, $P < 0.01$, four differential metabolites, such as N1-Methyl-2-pyridone-5-carboxamide (N1M2P5C), 1-Myristoyl-sn-glycerol-3-phosphocholine (MG3P), Caprylic acid (CA), and D-Xylulose (DX) were filtered out among MDR-TB/HC and MDR-TB/DS-TB (Figure 5). When N1M2P5C alone was used as a biomarker, the sensitivity, specificity, and accuracy of MDR-TB/DS-TB differential model were 90%, 56.7% and 0.758, respectively; and 50%, 76.7%, and

Table 3. Differential metabolites in MDR-TB group compared to DS-TB group and HC group.

ID	Name	MDR-TB/DS-TB			MDR-TB/HC			Column
		VIP	FC	*P*-value	VIP	FC	*P*-value	
1	Glycerophosphocholine	1.55	0.60	0.0196	2.53	0.49	0.0003	HILIC
2	N1-Methyl-2-pyridone-5-carboxamide	1.40	0.50	0.0002	1.46	1.50	0.0402	HILIC
3	1-Stearoyl-sn-glycerol 3-phosphocholine	1.59	0.75	0.0220	1.34	0.78	0.0202	HILIC
4	1-Myristoyl-sn-glycerol-3-phosphocholine	1.43	0.61	0.0061	1.65	0.58	0.0002	HILIC
5	1-Stearoyl-sn-glycerol	1.69	1.13	0.0363	2.33	1.26	0.0000	HILIC
6	1-Stearoyl-2-hydroxy-sn-glycerol-3-phosphocholine	1.08	0.71	0.0383	1.03	0.69	0.0000	HILIC
7	Tyramine	1.34	0.77	0.0009	2.08	0.84	0.0110	T3
8	L-Carnitine	1.17	0.81	0.0116	1.85	0.85	0.0357	T3
9	Caprylic acid	2.57	2.93	0.0000	2.57	3.06	0.0000	T3
10	D-Xylulose	2.85	8.27	0.0004	2.68	11.10	0.0002	T3
11	Taurochenodeoxycholate	1.22	2.10	0.0004	1.87	3.91	0.0002	T3
12	Inosine	2.52	3.25	0.0178	3.83	30.96	0.0004	T3
13	Deoxycholic acid	2.23	0.73	0.0033	1.55	0.60	0.0002	T3

FC: fold change.

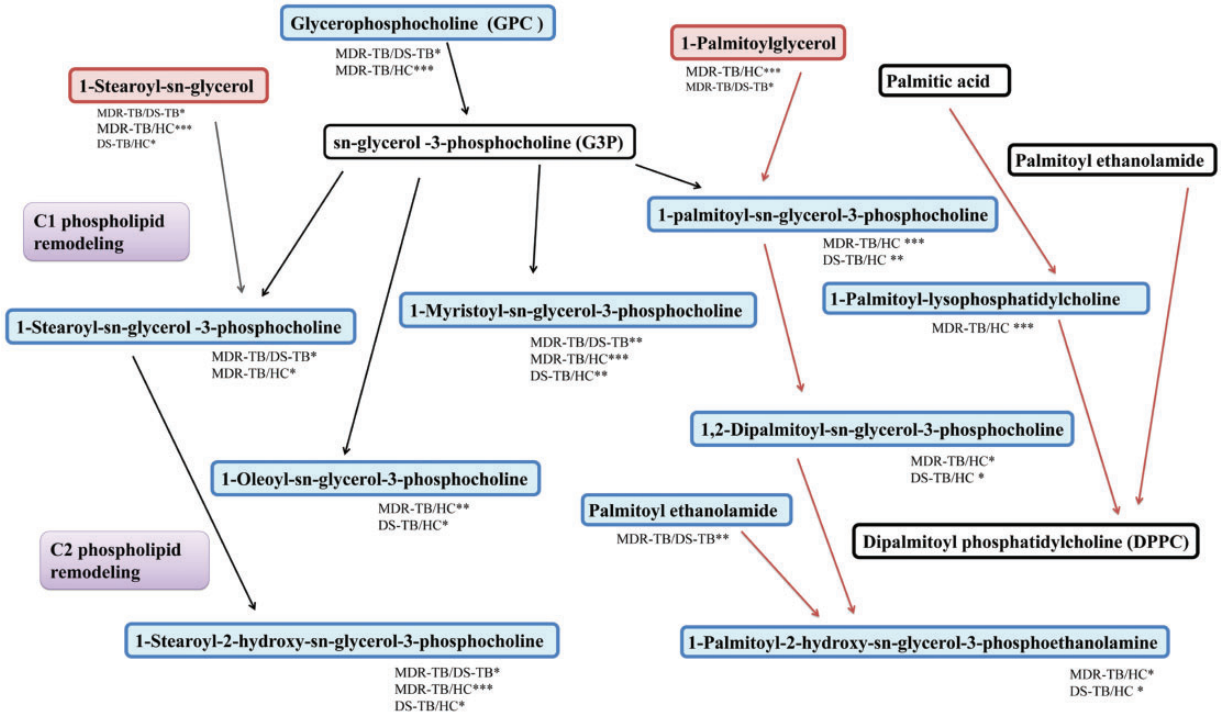

Figure 4. Diagram of differential metabolite enrichment pathways. The upward trend in metabolites was indicated by red rectangles, the downward trend in metabolites was indicated by blue rectangles, and the non-significant trend in metabolites was indicated by white rectangles. (A color version of this figure is available in the online journal.)

0.621 of MDR-TB/DS-TB differential model, respectively. When MG3P, CA, or DX were used as biomarkers alone, a similar performance was obtained (Figure 6, Table 4).

Multivariate logistic regression was used to analyze the effects of using the four differential metabolites in combination as the MDR-TB biomarker. The sensitivity, specificity, and accuracy of MDR-TB/DS-TB differential model were 86.7%, 86.7% and 0.928, respectively; and MDR-TB/HC differential model were 83.3%, 93.3%, and 0.892, respectively (Figure 6, Table 4). Its sensitivity and specificity were higher than that of any single metabolite and suggested that these metabolites could be combined as a potential biomarker for MDR-TB.

Discussion

Infectious drug-resistant MTB, improper drug regimen, inadequate course of treatment, intermittent medication are important causes of MDR-TB.[13] In 2017, approximately 68% of Chinese TB sputum-negative patients underwent diagnostic treatment without bacteriological confirmation and drug-resistance testing.[14] Improper diagnostic

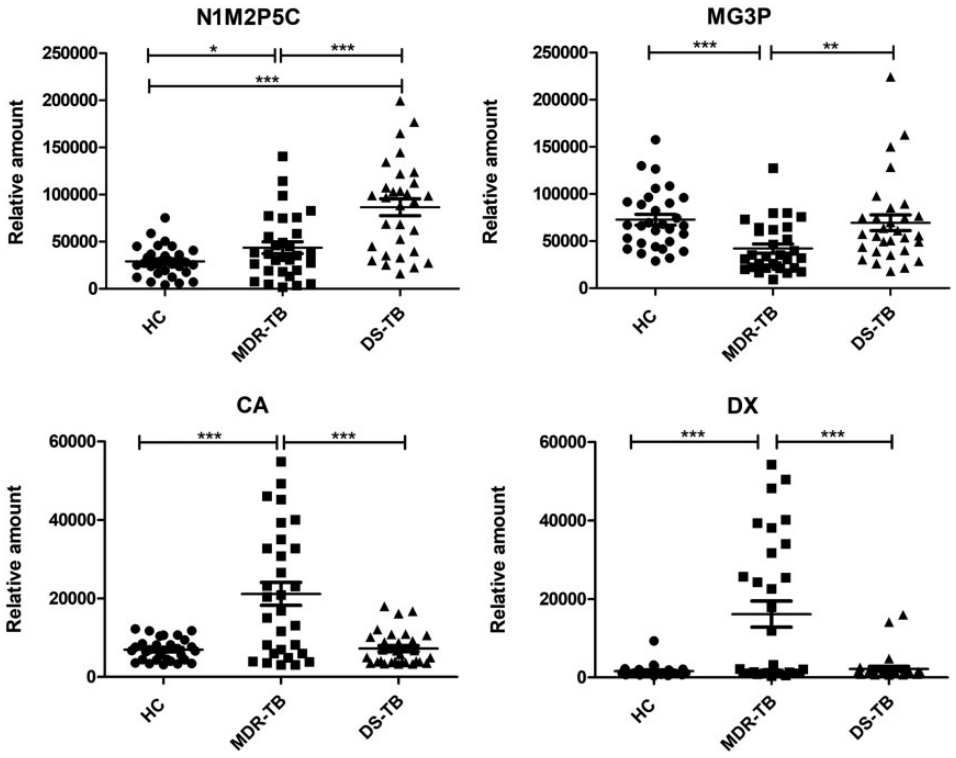

Figure 5. Relative quantitative values of differential metabolites N1M2P5C, MG3P, CA and DX. The *P*-value was tested by Student's *t*-test. $^{*}P < 0.05$; $^{**}P < 0.01$; $^{***}P < 0.001$.

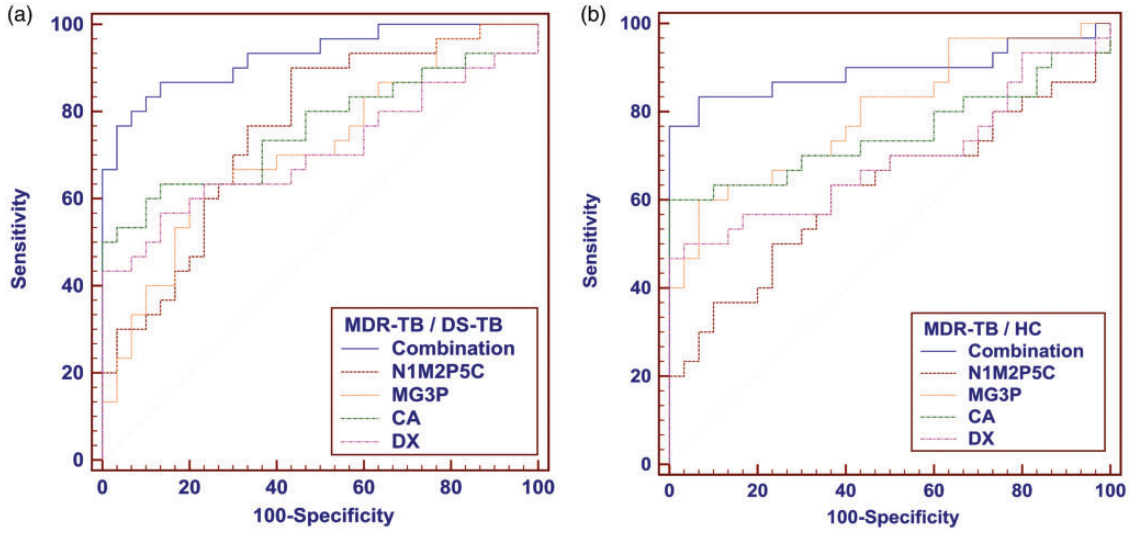

Figure 6. ROC analysis for differential metabolites N1M2P5C, MG3P, CA, DX and combinations. (a) the ROC analysis of MDR-TB/DS-TB group, (b) the ROC analysis of MDR-TB/HC group. (A color version of this figure is available in the online journal.)

treatment not only increases the risk of potential drug resistance but may also cause a declined drug efficacy, excessive side effects, resulting in decreased patient compliance and treatment shedding. In addition, China's labor force population is highly mobile, and the directly observed treatment short-course (DOTS) has not been strictly implemented, which has increased the source of the MDR-TB spreading.[15] Moreover, an epidemiological survey of China showed that the MDR-TB recurrence rate was approximately 61.3%, significantly higher than that of DS-TB (27.9%).[16] Therefore, the investigation of specific MDR-TB biomarkers is essential to enhance the early diagnostic efficiency and timely drug regimens adjustment in patients with MDR-TB.

Given the different affinities of each column for different chemical properties, the use of different types of columns may expand the range of detection for differential

Table 4. ROC analysis of N1M2P5C, MG3P, CA, DX, and the combinations.

	AUC	95%CI	Sensitivity%	Specificity%
Distinguishing MDR-TB from DS-TB				
Combination	0.928	0.905 to 0.999	86.7	86.7
1-Myristoyl-sn-glycerol-3-phosphocholine	0.714	0.583 to 0.824	63.3	76.7
N1-Methyl-2-pyridone-5-carboxamide	0.758	0.630 to 0.859	90.0	56.7
Caprylic acid	0.760	0.632 to 0.861	63.3	86.7
D-Xylulose	0.707	0.575 to 0.817	56.7	86.7
Distinguishing MDR-TB from HC				
Combination	0.892	0.825 to 0.977	83.3	93.3
1-Myristoyl-sn-glycerol-3-phosphocholine	0.798	0.674 to 0.890	60.0	93.3
N1-Methyl-2-pyridone-5-carboxamide	0.621	0.487 to 0.743	50.0	76.7
Caprylic acid	0.745	0.615 to 0.849	60.0	100.0
D-Xylulose	0.685	0.551 to 0.800	50.0	96.7

AUC: area under curve.

metabolites. The HILIC column and the T3 column are complementary in terms of the polarity and the pH range of the retained compound, and the elution order is reversed. This study used HILIC and T3 columns, compared to a single column, therefore it significantly increased the number of differential metabolites screened, reducing the omission of potential biomarkers. After multidimensional statistical analysis, four potential biomarkers of MDR-TB, N1M2P5C, MG3P, CA, and DX were obtained which were closely related to the pathophysiological changes of MDR-TB.

N1M2P5C is one of the metabolites of nicotinamide-adenine dinucleotide (NAD+) degradation. MTB can secrete TB necrosis toxin (TNT), hydrolyze the NAD+ of host cells, and initiate the necrotic apoptotic pathway, thereby evading the immunological killing effect of lysosomes.[17] In addition, isoniazid must be combined with the NAD+ of the host to synthesize the active conformation isonicotine-NADH to effectively resist mycobacteria.[18] Bhat *et al.*[19] and Vilcheze *et al.*[20] also found that effective treatment of isoniazid, pyrazinamide, rifampicin, and levofloxacin resulted in further accumulation of NADH in host macrophages. In this study, unlike DS-TB, metabolites of NADH were down-regulated in MDR-TB. We speculated the reason might be that MDR-MTB has a stronger TNT and could consume NAD+ faster, thereby accelerating apoptosis of macrophages to release more replicated MTB. As a result, there was not enough NADH to combine with drugs, resulting in the weakened anti-TB effect of the drug and eventually drug resistance. Thus, N1M2P5C might predict the sensitivity of MDR-TB patients to drugs.

MG3P is one of the phosphatidylcholines (PC) of the phospholipid remodeling derivative of sn-glycerol-3-phosphocholine (G3P) which constitutes the phospholipid bilayer of the cell membrane. In this study, many PC metabolites in TB showed a downward trend compared with that in the HC group, and the down-regulation was more significant in the MDR-TB group. Ramadurai *et al.*[21] found that anti-TB drugs such as rifampicin and levofloxacin could destroy the lipid bilayer membrane structure of host cells. Therefore, we speculated that cell membrane phospholipid remodeling in MDR-TB patients might be more active. More G3P might be consumed for the repair of lipid bilayers, maintaining membrane stability against drug penetration. In addition, in TB granuloma, the reductive stress caused by persistent hypoxia can affect the ion homeostasis of the cell membrane, causing the transmembrane potential to disappear.[22] It caused the PC to act as a second messenger for signal transduction and adhesion functions,[23] which in turn affected the interaction of the lipid membrane with the drug. Therefore, we speculated that PCs including MG3P might hinder bactericidal function of anti-TB drugs.

Caprylic acid (CA) is an important raw material for the synthesis of lipoic acid. Studies had shown that the proliferation of MTB is dependent on lipoate ester attachment groups synthesized from endogenously CA moiety. And the lipB of the octanoyl-[acyl carrier protein]-protein acyltransferase, encoding this pathway, was significantly up-regulated in MDR-TB.[24] In this study, MDR-TB showed a significant up-regulation of CA levels compared to DS-TB and HC, indicating increased CA synthesis in MDR-TB patients. In addition, high concentrations of CA have shown fatty acid toxicity and can cause membrane damage. Royce *et al.*[25] found that *E. coli* strains with high tolerance to CA exhibited better membrane fluidity and a relatively abundant membrane lipid structure. Therefore, we speculated that MDR-MTB might also have this type of enhanced resistance membrane. High concentrations of CA might be a characteristic metabolic mode by which MDR-MTB can exhibit resistance. So targeted blocking of the synthesis of lipoic acid linking groups in MDR-MTB might attenuate the resistance of MDR-MTB.

D-Xylulose (DX) is an intermediate of methylerythritol phosphate (MEP) pathway, a metabolite of 1-deoxy-d-xylulose-5-phosphate synthase (DXP). Two key enzymes were involved in this process, containing 1-deoxy-d-xylulose-5-phosphate reductoisomerase (DXR) and 1-deoxy-d-xylulose-5-phosphate synthase (DXS). MTB relies solely on the MEP pathway to produce dimethylallyl pyrophosphate (DMAPP) and its isomer isopentenyl pyrophosphate (IPP).[26] Many secondary metabolites of IPP and DMAPP are involved in the changes in MTB membrane properties, electron transport in the respiratory chain, and synthesis of polyprenyl phosphates that are critical for the MTB cell wall.[27] In this study, MDR-TB showed a significant up-regulation of DX levels compared to DS-TB and HC. We speculated that the MEP pathway of MDR-MTB was

more active, thereby enhancing the viability and resistance of the strain. In addition, due to the complete absence of the MEP pathway in human metabolism, studies had shown that DXS and DXR inhibitors have huge potential for resistance to a wide spectrum of bacteria.[28,29] Therefore, we speculated that DXS and DXR might be promising new targets for anti-MDR-TB drugs.

Our study also found that the metabolites of DPPC, the main component of pulmonary surfactant were down-regulated in TB patients compared to HC. In spite of no statistically significant difference, the results of MDR-TB compared to DS-TB showed a downward trend. Dodd *et al*. found that pulmonary surfactant-active lipids could be actively taken up by MTB-infected macrophages through the scavenger receptor CD36. Meanwhile, they could inhibit TLR2-mediated TNFα production in host cells and impair the autoimmune bactericidal effect of the host.[30] In addition, the inhaled anti-TB drugs have been developed, which can avoid the first-pass elimination, thereby improving the drug utilization rate. However, there are no reports of pulmonary surfactant-coated lipid-inhaled anti-TB drugs. We speculated that the self-uptake of pulmonary surfactant lipids by infected MTB macrophages may be one of the prospects for improving MDR-TB therapy.

In conclusion, the four metabolites identified in this study showed abnormal abundance in MDR-TB and might collectively reflect the viability of MDR-MTB and the ability to resist sterilization. The accuracy, sensitivity, and specificity of the combined MDR-TB/DS-TB differential model built from the four differential metabolites were 0.928, 86.7%, and 86.7%, respectively. It suggested that MG3P, N1M2P5C, DX, CA might be potential biomarkers of MDR-TB. Our study provided experimental basis for understanding the MDR-TB pathogenesis. It also pointed out a molecular biology research direction for the design of novel anti-MDR-TB drugs.

Authors' contributions: JCL designed this study. HH coped with the experiments. YSH and HH arranged the figures. JC, LYS, LLW, HH, HHT, TTJ, WJY and ZBL collected blood samples and clinical data from the subjects. JCL and HH established mathematical models and completed this manuscript.

ACKNOWLEDGEMENTS

The authors thank Dr. Zheng-Jiang Li at the First Affiliated Hospital of Jiaxing University for collecting blood samples and all participants in this study.

DECLARATION OF CONFLICTING INTERESTS

The author(s) declared that there were no potential conflicts of interest in the article's research, authorship, and publication.

ETHICAL APPROVAL

The study was in compliance with Declaration of Helsinki principle and was approved by the Ethics Committee of school of medicine of Zhejiang University (China). Informed consent was received before blood sample were collected.

FUNDING

The author(s) disclosed receipt of the following financial support for the research, authorship, and/or publication of this article: This work was supported by grants from Natural Science Foundation of Guangdong Province [grant number 2017A030311014], National Natural Science Foundation of China [grant number 81772266], and Guangzhou Science and Technology Project [grant number 201804010369], and the Key Construction Foundation of Guangdong High-level Hospital.

ORCID iDs

Huai Huang https://orcid.org/0000-0002-8978-7043
Ji-Cheng Li https://orcid.org/0000-0002-9631-8931

SUPPLEMENTAL MATERIAL

Supplemental material for this article is available online.

REFERENCES

1. Organization. WH. Global tuberculosis report 2018. World Health Organization Web Site, www.who.int/tb/publications/global_report/en/ (accessed 30 October 2018)
2. Nguyen TNA, Anton-Le Berre V, Bañuls A-L, Nguyen T. Molecular diagnosis of drug-resistant tuberculosis. *Front Microbiol* 2019;**10**:794
3. Dorman SE, Schumacher SG, Alland D, Nabeta P, Armstrong DT, King B, Hall SL, Chakravorty S, Cirillo DM, Tukvadze N, Bablishvili N, Stevens W, Scott L, Rodrigues C, Kazi MI, Joloba M, Nakiyingi L, Nicol MP, Ghebrekristos Y, Anyango I, Murithi W, Dietze R, Lyrio Peres R, Skrahina A, Auchynka V, Chopra KK, Hanif M, Liu X, Yuan X, Boehme CC, Ellner JJ, Denkinger CM. Xpert MTB/RIF ultra for detection of *Mycobacterium tuberculosis* and rifampicin resistance: a prospective multicentre diagnostic accuracy study. *Lancet Infect Dis* 2018;**18**:76–84
4. Wang C, Liu CM, Wei LL, Shi LY, Pan ZF, Mao LG, Wan XC, Ping ZP, Jiang TT, Chen ZL, Li ZJ, Li JC. A group of novel serum diagnostic biomarkers for Multidrug-Resistant tuberculosis by iTRAQ-2D LC-MS/MS and solexa sequencing. *Int J Biol Sci* 2016;**12**:246–56
5. Beger RD, Dunn W, Schmidt MA, Gross SS, Kirwan JA, Cascante M, Brennan L, Wishart DS, Oresic M, Hankemeier T, Broadhurst DI, Lane AN, Suhre K, Kastenmuller G, Sumner SJ, Thiele I, Fiehn O. Kaddurah-Daouk R. Metabolomics enables precision medicine: "a white paper, community perspective". *Metabolomics* 2016;**12**:149
6. Hodgson AB, Randell RK, Mahabir-Jagessar TK, Lotito S, Mulder T, Mela DJ, Jeukendrup AE, Jacobs DM. Acute effects of green tea extract intake on exogenous and endogenous metabolites in human plasma. *J Agric Food Chem* 2014;**62**:1198–208
7. Dunn WB, Bailey NJ, Johnson HE. Measuring the metabolome: current analytical technologies. *Analyst* 2005;**130**:606–25
8. Wang W, Zhang W, Liu J, Sun Y, Li Y, Li H, Xiao S, Shen X. Metabolomic changes in follicular fluid induced by soy isoflavones administered to rats from weaning until sexual maturity. *Toxicol Appl Pharmacol* 2013;**269**:280–9
9. Forsberg EM, Huan T, Rinehart D, Benton HP, Warth B, Hilmers B, Siuzdak G. Data processing, multi-omic pathway mapping, and metabolite activity analysis using XCMS online. *Nat Protoc* 2018;**13**:633–51
10. China. NHCotPsRo. Diagnostic criteria for pulmonary tuberculosis. National Health Commission of the People's Republic of China, www.nhcgovcn/ewebeditor/uploadfile/2017/12/20171212154852389pdf (accessed 9 November 2017)
11. Dunn WB, Broadhurst D, Begley P, Zelena E, Francis-McIntyre S, Anderson N, Brown M, Knowles JD, Halsall A, Haselden JN, Nicholls AW, Wilson ID, Kell DB, Goodacre R. Procedures for large-scale metabolic profiling of serum and plasma using gas

chromatography and liquid chromatography coupled to mass spectrometry. *Nat Protoc* 2011;**6**:1060–83
12. Wang J, Zhang T, Shen X, Liu J, Zhao D, Sun Y, Wang L, Liu Y, Gong X, Liu Y, Zhu Z-J, Xue F. Serum metabolomics for early diagnosis of esophageal squamous cell carcinoma by UHPLC-QTOF/MS. *Metabolomics* 2016;**12**:116
13. Pradipta IS, Van't Boveneind-Vrubleuskaya N, Akkerman OW, Alffenaar JWC, Hak E. Predictors for treatment outcomes among patients with drug-susceptible tuberculosis in The Netherlands: a retrospective cohort study. *Clin Microbiol Infect* 2019;**25**:761.e1–761.e7
14. Huang F, van den Hof S, Qu Y, Li Y, Zhang H, Wang L, Sun M, Lu W, Hou S, Zhang T, Huan S, Chin DP, Cobelens F. Added value of comprehensive program to provide universal access to care for sputum smear-negative drug-resistant tuberculosis, China. *Emerging Infect Dis* 2019;**25**:1289–96
15. Koch A, Cox H, Mizrahi V. Drug-resistant tuberculosis: challenges and opportunities for diagnosis and treatment. *Curr Opin Pharmacol* 2018;**42**:7–15
16. Sun Y, Harley D, Vally H, Sleigh A. Impact of multidrug resistance on tuberculosis recurrence and Long-Term outcome in China. *PLoS One* 2017;**12**:e0168865
17. Sun J, Siroy A, Lokareddy RK, Speer A, Doornbos KS, Cingolani G, Niederweis M. The tuberculosis necrotizing toxin kills macrophages by hydrolyzing NAD. *Nat Struct Mol Biol* 2015;**22**:672–8
18. Rozwarski DA, Grant GA, Barton DH, Jacobs WR, Jr., Sacchettini JC. Modification of the NADH of the isoniazid target (InhA) from *Mycobacterium tuberculosis*. *Science* 1998;**279**:98–102
19. Bhat SA, Iqbal IK, Kumar A. Imaging the NADH:NAD(+) homeostasis for understanding the metabolic response of mycobacterium to physiologically relevant stresses. *Front Cell Infect Microbiol* 2016;**6**:145
20. Vilcheze C, Weisbrod TR, Chen B, Kremer L, Hazbon MH, Wang F, Alland D, Sacchettini JC, Jacobs WR. Jr., Altered NADH/NAD+ ratio mediates coresistance to isoniazid and ethionamide in mycobacteria. *Antimicrob Agents Chemother* 2005;**49**:708–20
21. Ramadurai S, Sarangi NK, Maher S, MacConnell N, Bond AM, McDaid D, Flynn D, Keyes TE. Microcavity-supported lipid bilayers; evaluation of Drug-Lipid membrane interactions by electrochemical impedance and fluorescence correlation spectroscopy. *Langmuir* 2019;**35**:8095–109
22. Tokes T, Tuboly E, Varga G, Major L, Ghyczy M, Kaszaki J, Boros M. Protective effects of L-alpha-glycerylphosphorylcholine on ischaemia-reperfusion-induced inflammatory reactions. *Eur J Nutr* 2015;**54**:109–18
23. Nunes C, Brezesinski G, Lopes D, Lima JL, Reis S, Lucio M. Lipid-drug interaction: biophysical effects of tolmetin on membrane mimetic systems of different dimensionality. *J Phys Chem B* 2011;**115**:12615–23
24. Ma Q, Zhao X, Nasser Eddine A, Geerlof A, Li X, Cronan JE, Kaufmann SH, Wilmanns M. The *Mycobacterium tuberculosis* LipB enzyme functions as a cysteine/lysine dyad acyltransferase. *Proc Natl Acad Sci U S A* 2006;**103**:8662–7
25. Royce LA, Yoon JM, Chen Y, Rickenbach E, Shanks JV, Jarboe LR. Evolution for exogenous octanoic acid tolerance improves carboxylic acid production and membrane integrity. *Metab Eng* 2015;**29**:180–8
26. Eoh H, Brennan PJ, Crick DC. The *Mycobacterium tuberculosis* MEP (2C-methyl-d-erythritol 4-phosphate) pathway as a new drug target. *Tuberculosis* 2009;**89**:1–11
27. Wang X, Dowd CS. The methylerythritol phosphate pathway: promising drug targets in the fight against tuberculosis. *ACS Infect Dis* 2018;**4**:278–90
28. Leon A, Liu L, Yang Y, Hudock MP, Hall P, Yin F, Studer D, Puan KJ, Morita CT, Oldfield E. Isoprenoid biosynthesis as a drug target: bisphosphonate inhibition of *Escherichia coli* K12 growth and synergistic effects of fosmidomycin. *J Med Chem* 2006;**49**:7331–41
29. Dhiman RK, Schaeffer ML, Bailey AM, Testa CA, Scherman H, Crick DC. 1-Deoxy-D-xylulose 5-phosphate reductoisomerase (IspC) from *Mycobacterium tuberculosis*: towards understanding mycobacterial resistance to fosmidomycin. *J Bacteriol* 2005;**187**:8395–402
30. Dodd CE, Pyle CJ, Glowinski R, Rajaram MV, Schlesinger LS. CD36-Mediated uptake of surfactant lipids by human macrophages promotes intracellular growth of *Mycobacterium tuberculosis*. *J Immunol* 2016;**197**:4727–35

(Received October 10, 2019, Accepted January 10, 2020)